

Pickles on FIRE: The 3D Shape Evolution of Simulated Milky Way–Mass Galaxies

LUKE Y. XIA ¹, COURTNEY KLEIN ¹, JAMES BULLOCK ¹, MICHAEL BOYLAN-KOLCHIN ², VINCENT CAUDILLO ¹,
JORGE MORENO ^{3,4}, FRANCISCO J. MERCADO ^{3,5} AND ROBERT FELDMANN ⁶

¹*Department of Physics and Astronomy, University of California Irvine, Irvine, CA 92697, USA*

²*Department of Astronomy, The University of Texas at Austin, Austin, TX 78712, USA*

³*Department of Physics and Astronomy, Pomona College, Claremont, CA 91711, USA*

⁴*Carnegie Observatories, Pasadena, CA 91101, USA*

⁵*TAPIR, California Institute of Technology, Pasadena, CA 91125, USA*

⁶*Institute for Computational Science, University of Zurich, Zurich CH-8057, Switzerland*

ABSTRACT

JWST and HST observations have revealed numerous elongated, pickle-shaped galaxies at high to intermediate redshifts, with masses close to those expected for Milky Way progenitors. Here we use reduced-mass eigentensors to quantify the ellipsoidal shape evolution of thirteen Milky Way-mass galaxies simulated using FIRE-2 physics; all but one form disks at $z = 0$. We find that all of our Milky Way progenitors go through phases when they are elongated. They often oscillate between spheroidal and elongated shapes in the early Universe over billion-year timescales. This is true whether we measure shapes weighted on stellar mass or luminosity, though the luminosity shapes show more extreme elongation and variance. In contrast, the stellar populations of our $z = 0$ Milky Way analogs are never elongated and always symmetric about their minor axes. The youngest stars at $z = 0$ reside in thin disks, intermediate-age stars reside in thick disks, and the oldest stars reside in flattened spheroids that are symmetric about their minor axes. Despite their symmetric shapes at $z = 0$, the old and intermediate age stellar populations were often arranged in the shape of elongated pickles or triaxial spheroids at the time they formed, meaning that these populations changed shape significantly over time. Our results suggest that observed elongated galaxies seen in the early Universe are not stable structures, but rather reflect transitory phases of galaxy evolution.

1. INTRODUCTION

The origin and evolution of the three-dimensional structure of galaxies is among the core questions in galactic astrophysics (Hubble 1926; Sandage et al. 1970; Binney & de Vaucouleurs 1981; Conselice 2014; Favaro et al. 2025). Galaxy shapes are fundamental to our understanding of the Universe and offer important tests for modern theories of galaxy formation (White & Rees 1978; Blumenthal et al. 1984; Springel et al. 2005; Somerville & Davé 2015; Arora et al. 2025; Vargya et al. 2022).

The Milky Way provides a powerful window into galactic structure (Jurić et al. 2008; Haywood et al. 2013; Bovy et al. 2016). We know, for example, that the youngest Milky Way stars reside within a flattened disk and that older stars are more isotropically distributed. However, relating the shape distribution of the oldest stars today to the shape of the Galaxy at the time when those stars were forming is non-trivial owing to the possibility of dynamical phase mixing and relaxation (Merritt & Valluri 1996). For this reason, a detailed under-

standing of the assembly of Milky Way–type galaxies must be informed by theoretical models combined with empirical studies of Milky Way–like progenitors in the distant Universe.

For the vast majority of galaxies, we must observationally infer information about their 3D shapes using their 2D projections on the sky. Under the assumption that galaxies are well-approximated by triaxial ellipsoids (Binney 1978), it is possible to infer their 3D properties statistically using observed 2D axis ratios of galaxy populations (Sandage et al. 1970; Fasano & Vio 1993; Ryden 2004). Under the ellipsoidal approximation, we can think of galaxies as falling within three broad categories: spheroidal (all three axes roughly equal, like an orange), disk (flattened in one direction, like a pancake), or elongated (flattened in two directions, like a pickle).

By examining projected axis distributions, observational studies have concluded that the majority of massive quenched galaxies in the local Universe are spheroidal and that massive star-forming galaxies at

$z = 0$ are usually disks like the Milky Way (Lambas et al. 1992; Padilla & Strauss 2008; de Nicola et al. 2022). At lower masses, the situation is somewhat more ambiguous: most studies suggest that low-mass galaxies at $z = 0$ are a mixture of oblate disks and spheroids (Ichikawa 1989; Binggeli & Popescu 1995; Sung et al. 1998; Roychowdhury et al. 2013; Putko et al. 2019; Kado-Fong et al. 2020; Rong et al. 2020), while others have found that a substantial population of local galaxies in this regime may be elongated or prolate in shape (Vincent & Ryden 2005; Burkert 2017).

At higher redshifts, galaxies are known to exhibit more irregular, clumpy morphologies than we see in the local Universe (e.g. Elmegreen et al. 2005, 2007; Förster Schreiber et al. 2009). Of particular interest is the work of van der Wel et al. (2014), who studied the shapes of star-forming galaxies from $z = 0 - 2.5$ and found that the fraction of systems that are elongated increases toward higher redshifts and lower masses. For example, at $z \simeq 1$ ($z \simeq 2$) they found that the population of $M_\star \simeq 10^9 M_\odot$ ($10^{10} M_\odot$) galaxies is evenly divided between those that are elongated and those that are disk-like. These conclusions are consistent with previous work (Ferguson et al. 2004; Ravindranath et al. 2006; Yuma et al. 2011) suggesting that low-mass galaxies at high redshifts are elongated. Zhang et al. (2019) used CANDELS data to show that star-forming galaxies tend to be elongated at low stellar mass and high redshift and disk-like at high stellar mass and low redshift, in qualitative agreement with van der Wel et al. (2014).

More recently, Pandya et al. (2024) used JWST data to study the shapes of star-forming galaxies from $z = 0.5 - 8$, and found that many galaxies at $z > 1$ with masses consistent with them being progenitors of L_\star galaxies today are elongated in shape. Specifically, they find that the fraction of $M_\star = 10^{9-9.5} M_\odot$ galaxies that are prolate is $\sim 40\%$ at $z = 1$ and that this fraction increases to $\sim 50 - 80\%$ at $z = 3 - 8$.

In related work, Vega-Ferrero et al. (2024) used a machine learning method trained on TNG50 simulations to classify galaxies observed with JWST and found that a substantial fraction of galaxies that could be naively classified as disks may be intrinsically elongated. Prior to this, Ceverino et al. (2015) and Tomassetti et al. (2016) showed that $\sim 10^9 M_\odot$ galaxies at $z \sim 2$ in their simulations are often prolate and live in dark matter halos that are themselves elongated in the same direction as the stellar distribution. This mass range is roughly what is expected for the mass of the main progenitor of Milky Way size systems at $z = 0$ (e.g. Sotillo-Ramos et al. 2022).

These results raise a question: Did most Milky Way-size galaxies go through a phase of evolution when their stars were forming in elongated shapes? In this paper, we look specifically at the shape evolution history of Milky Way-like galaxies using a set of 13 zoom-in FIRE-2 (Hopkins et al. 2018) simulations. We characterize galaxy shapes using triaxial ellipsoids and measure the axis ratios for all stars, young stars, luminosity-weighted stars, and dark matter at multiple epochs. We also measure the shapes of mono-age populations of stars at $z = 0$ and relate them to the shapes that those stars had at the time of their birth.

In Section 2 we discuss our simulations and how the shapes are measured, in Section 3 we discuss our results, in Section 4 we discuss our conclusions.

2. METHODS

2.1. Simulations

Our simulations were performed as part of the Feedback in Realistic Environments (FIRE) project¹ and specifically use the FIRE-2 set of feedback prescriptions (Hopkins et al. 2018). In short, the simulations use the code GIZMO², with hydrodynamics solved using the mesh-free Lagrangian Godunov “MFM” method. The runs include cooling and heating from a uniform, evolving ionizing background (Faucher-Giguère et al. 2009) and local stellar sources from $T \sim 10 - 10^{10}$ K; star formation occurs in locally self-gravitating, dense, self-shielding, molecular, Jeans unstable gas. Simulations also include feedback from OB & AGB mass-loss, SNe Ia & II, and multi-wavelength photo-heating and radiation pressure with inputs taken directly from stellar evolution models.

In this paper, we analyze the 3D geometry of 13 simulated galaxies, all of which reach a mass similar to that of the Milky Way at $z = 0$. Seven of these are part of the Latte suite (Wetzel et al. 2016; Garrison-Kimmel et al. 2017; Hopkins 2017; Garrison-Kimmel et al. 2019a) and six are part of the “ELVIS on FIRE” project, which were simulated in pairs similar to the Milky Way and M31 (Garrison-Kimmel et al. 2019a,b). Other than the ELVIS runs being associated with Local-Group like pairs, the main difference is that the Latte suite is run with initial baryonic particle masses $\sim 7000 M_\odot$ that are about twice as large as those in the ELVIS suite, $\sim 3500 M_\odot$. More details of these simulations can be found in the associated references above.

¹ <http://fire.northwestern.edu>

² <http://www.tapir.caltech.edu/~phopkins/Site/GIZMO.html>

2.2. Measuring and Characterizing Simulated Galaxy Shapes

Axis ratios of stars in simulated galaxies have been calculated with a variety of methods including 3D isodensity surfaces, mass eigentensors, or minimum-volume-enclosing ellipsoids (e.g. Ceverino et al. 2015; Tomassetti et al. 2016; Thob et al. 2019; Zhang et al. 2022; Valenzuela et al. 2024; Keith et al. 2025). In this work, we adopt a shape tensor approach (e.g. Bailin & Steinmetz 2005; Allgood et al. 2006) and specifically use a reduced mass eigentensor (Chua et al. 2019; Klein et al. 2025):

$$S_{ij} = \frac{\sum_n r_{\text{ell},n}^{-2} m_n x_{n,i} x_{n,j}}{\sum_n m_n}, \quad (1)$$

with the indices i and j each running over the three spatial dimensions and the sum covering $n = 1, 2, \dots, N$ star particles within the volume of choice (see below). The quantity m_n represents the star particle’s mass, and $x_{n,i}$, $x_{n,j}$ are pairs of coordinate distances in the i and j directions. Diagonalizing the tensor yields eigenvalues $\lambda_1 \geq \lambda_2 \geq \lambda_3$, from which the axis lengths may be associated as $A, B, C \propto \sqrt{\lambda_1}, \sqrt{\lambda_2}, \sqrt{\lambda_3}$. Important in our analysis is the quantity $r_{\text{ell},n}^{-2}$, which allows us to weigh each star particle inversely with its elliptical distance from the galaxy center:

$$r_{\text{ell}} = \sqrt{x^2 + \frac{y^2}{(B/A)^2} + \frac{z^2}{(C/A)^2}}. \quad (2)$$

Here, A, B, C represent the axis lengths of the current iteration. Without this weighting, particles with large radii within the volume tend to drive inferred shapes to be more spherical, limiting the dynamic range of the associated axis ratios. This aligns with work by Valenzuela et al. (2024), which finds that this weighting provides a strong measurement for the shape of a galaxy within a boundary.

We calculate galaxy shapes iteratively by first considering all star particles within a spherical volume of radius equal to one tenth of the host halo virial radius³, $A = B = C = 0.1 r_{\text{vir}}$. The reduced mass eigentensor S_{ij} gives us an initial set of eigenvectors $\vec{A}, \vec{B}, \vec{C}$ and eigenvalues $\lambda_1, \lambda_2, \lambda_3$. The rotation matrix R^{-1} is used to rotate the galaxy from the simulation axes to the new eigenbasis, where $R = [\vec{A}, \vec{B}, \vec{C}]$. In the first iteration, the square roots of the eigenvalues are scaled so that the largest value matches the distance from the center to the farthest star particle in the volume. This

³ We define the virial mass and radius of our galaxies following the definition in Bryan & Norman (1998). Note that the virial radius evolves with time for any particular galaxy.

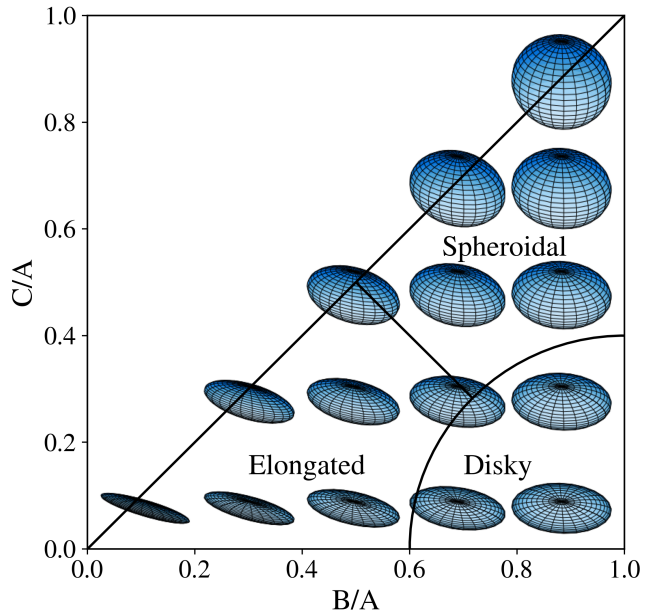


Figure 1. A sample of ellipsoids that demonstrate the meaning of our C/A and B/A parameter space, where $C < B < A$. The defined regions for diskly, spheroidal, and elongated shapes are indicated in the figure.

produces a new set of principal axes $\vec{A}', \vec{B}', \vec{C}'$. After the first iteration, we scale the lengths of the axes by a factor of $(A'B'C'/ABC)^{1/3}$ to preserve volume. This process is repeated until the axis ratios B/A and C/A converge to within 10^{-4} of the previous iteration. To precisely define the final 3D ellipsoidal shape, extraneous particles are excluded by scaling the ellipsoid down until it retains 90% of its original mass. This adjustment minimally affects the shape due to the factor r_{ell}^2 in the denominator. We define the stellar mass of each galaxy as the total stellar mass within this ellipsoidal volume.

Following Zhang et al. (2019), we categorize galaxies into elongated, diskly, and spheroidal shapes based on their relative axis ratios C/A and B/A . Figure 1 illustrates how we separate galaxies into each of these categories. Idealized ellipsoids are depicted as examples for comparison.

2.3. Shape Weighting

We measure the shapes of different populations and weightings of stars within our galaxies to understand their shape evolution. First, we study each of our galaxies at $z = 0$ and measure the shapes of stellar populations in different age bins. For the remainder of the paper, this will be referred to as the “archaeological” approach, since it excavates the past of the galaxy from the present-day distribution of its stars. Second, we track the main progenitor of each galaxy back in time and

measure the stellar shape distributions of 1) all stars, 2) young stars, 3) all stars weighted by their luminosities, 4) all dark matter particles within the same volume. For young stars, we focus on stars with ages less than 500 Myr.⁴ For the luminosity-weighted approach, we replace the particle mass m_n in Equation 1 with its g -band luminosity L_n . This is a quasi-observable shape measurement; however, measurements of observed galaxies are projected and affected by dust and other factors.

Finally, we employ our algorithm to measure the shape of the dark matter structure within both our standard volume ($0.1r_{\text{vir}}$) and an extended radius of r_{vir} using dark matter particles rather than star particles in Equation 1. Thus, each of the 13 simulations is measured using all methods in 18 different snapshots, spaced approximately 750 Myr apart, starting from $z = 7$ to $z = 0$. In this context, we refer to the lookback time of a population as the time between a given snapshot and the present day ($z = 0$); for example, $z = 7$ corresponds to a lookback time of 13.0 Gyr.

2.4. Measurement Accuracy

Measuring the shapes of our galaxies accurately at $z = 0$ is fairly straightforward because each simulation contains millions of star particles. However, as we examine subsets of particles in progenitor galaxies at earlier times, the particle count declines rapidly. We perform the following experiment to assess the minimum number of particles required to accurately measure the shape of a system. We first measured the shapes of several highly-resolved galaxies at $z = 0$ within $0.1r_{\text{vir}}$ and recorded this as their “true” shape. We then progressively removed fractions of particles and analyzed the deviations in the resulting shape measurements. For each fraction, we removed a random subset of particles and recalculated the shape 100 times to quantify the deviation. We increased the fraction of star particles removed until the standard deviation in derived axis ratios, divided by the “true” shape, exceeded 0.05. Our findings indicate that this threshold was consistently exceeded when fewer than 1,000 particles remained. Thus, we adopt a lower limit of 1,000 particles as the minimum necessary to reliably measure the galaxy’s shape.⁵

⁴ We have looked at stars younger than 100 Myr and find similar results, but the 500 Myr age range provides consistently enough star particles (1000) to measure shapes accurately at all lookback times considered, as discussed in Section 2.4.

⁵ In practice, the need for 1,000 particles is what motivated us to chose a 500 Myr cutoff for stars we classify as “young”. A younger age limit would have resulted in fewer stars at some of our higher redshift timesteps.

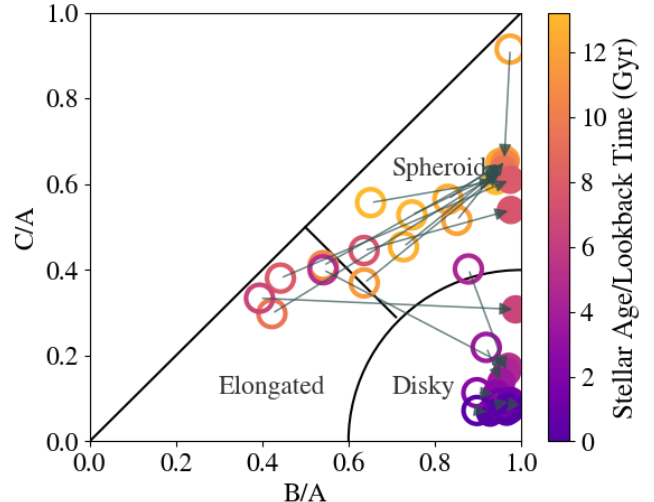


Figure 2. Shapes of Thelma’s stellar populations at formation (open) and at $z = 0$ (filled), binned by age, in the parameter space introduced in Figure 1. An arrow connects each stellar population shape at formation to its shape at the present day. The color bar maps to stellar age (or, equivalently, lookback time to their formation). We see that early times, young stars often resided in elongated or triaxial-spheroidal configurations when they formed. The shapes of the same populations today are much “rounder” or symmetric about their short axes, with $B/A \sim 0.9$.

3. RESULTS

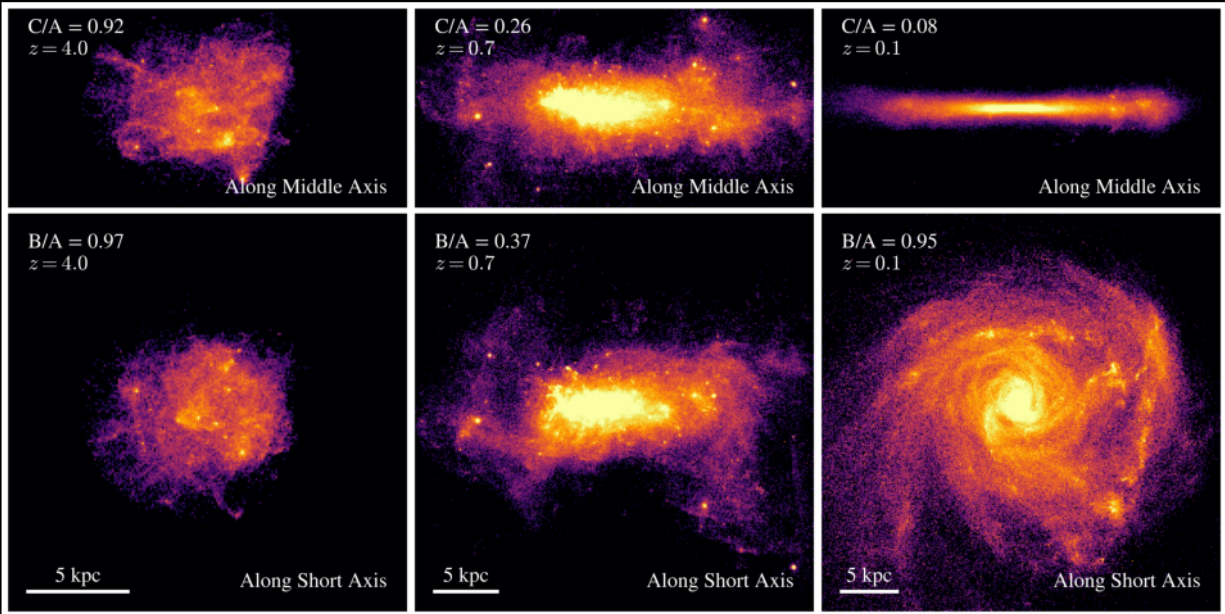
In what follows, we first present shape evolution results for a single simulated galaxy, Thelma, and in the following subsection we discuss sample-wide results. We begin with a single galaxy for the sake of clarity. Thelma is fairly typical of the galaxies in our suite in that it forms a prominent disk at $z = 0$. There is nothing particularly unique about this galaxy.

3.1. Case Study: Thelma

Figure 2 presents the evolution of the shapes of individual stellar populations in Thelma. The shapes are tracked in the shape parameter space (C/A vs. B/A) introduced in Figure 1.

The open circles in Figure 2 show the axis ratios of young stellar populations (< 500 Myr) in the main progenitor of Thelma at various snapshots. The points are colored by the lookback time of the snapshot and are mapped to the color bar on the right. The shapes of the same stellar populations at $z = 0$ are shown by solid points. The solid points use the same color scheme, now interpreted as stellar age at $z = 0$. The shapes at formation (open) are connected to the shapes at $z = 0$ (solid) by gray arrows. We see that at late times (< 4 Gyr lookback) young stars tend to inhabit disk configurations.

Young Stars at Time of Formation



Where They Are Now

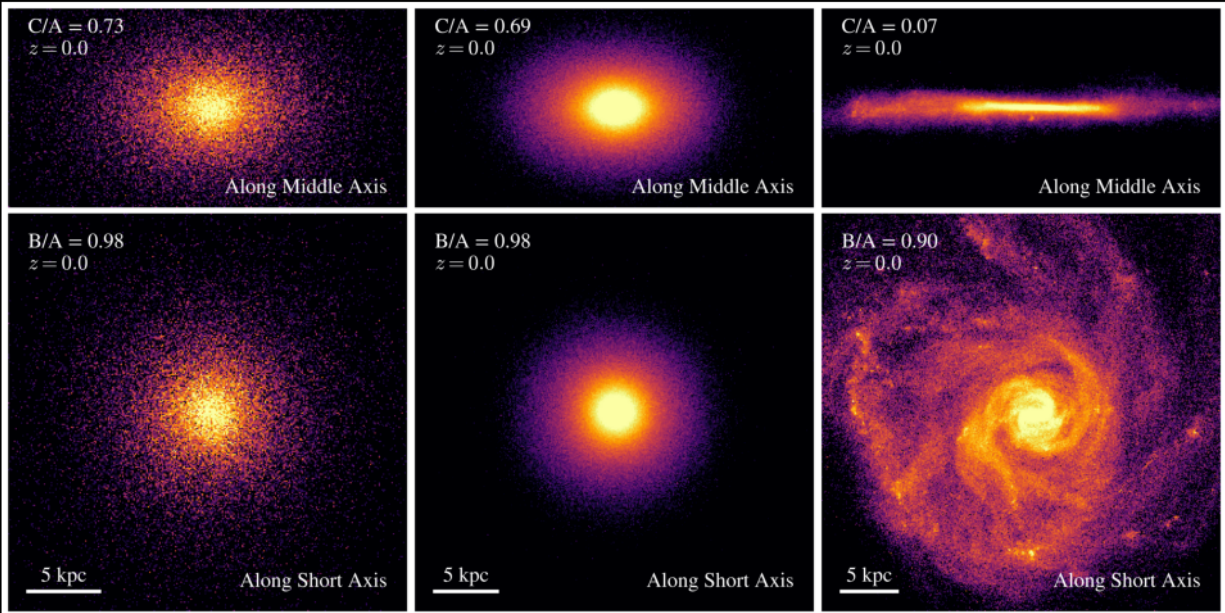


Figure 3. Density projections of stellar populations younger than 500 Myr near their times of formation (top set) and at $z = 0$ (bottom set). In the top set of images, we show middle and short-axis projections of young stars at $z = 4.0$ (left, 12.2 Gyr lookback), $z = 0.7$ (middle, 6.4 Gyr lookback), and $z = 0.1$ (bottom, 1.3 Gyr lookback). The bottom set of images shows the same stars, now at $z = 0$, along the same respective axis orientations (though the axes are calculated separately at $z = 0$). We see that the initially spheroidal population (left) evolves into a spheroidal shape at $z = 0$. The elongated stellar population (middle) at $z = 0.7$ has evolved into a flattened spheroid over the past 6.4 Gyr. The stars that formed in a thin disk at $z = 0.1$, or 1.30 Gyr ago (right), still remain in a thin disk today. Regardless of their initial shapes, in all cases the $z = 0$ populations are quite symmetric (circular) in short-axis projections.

urations and that these stars tend to remain in disk shapes at $z = 0$. However, young stars are often arranged in elongated or triaxial/spheroidal configurations at lookback times greater than ~ 4 Gyr. Moreover, the same stellar populations wind up with drastically different shapes at $z = 0$. In almost every case, stars relax to become much more symmetric about their minor axis ($B/A \simeq 0.9$) and never evolve into elongated configurations at $z = 0$. Also of interest is that at intermediate lookback times ($\sim 4 - 6$ Gyr) some of the initially elongated configurations evolve into axisymmetric disks, while most of the elongated configurations (which occurred slightly earlier, $\sim 6 - 8.5$ Gyr ago) evolve into axisymmetric spheroidal shapes.

An example visualization of this kind of evolution in shape is provided in Figure 3. The top panels show 2D density maps of young stars near the time of their birth and the bottom panels show the same populations at $z = 0$. Specifically, the top set of panels shows the middle axis (upper) and short axis (lower) orientations of young stars in Thelma at $z = 4$ (left), $z = 0.7$ (middle) and $z = 0.1$ (right). The lookback times correspond to 12.2 Gyr, 6.4 Gyr, and 1.3 Gyr, respectively. The bottom panels show the same stars at $z = 0$, oriented along their $z = 0$ middle and short axes. Of particular note is that, while the young stars at $z = 0.7$ were arranged as an elongated “pickle”, those stars evolve into a flattened spheroidal shape at $z = 0$. In contrast, the population of young stars at $z = 4.0$ is spheroidal in shape both at formation and at $z = 0$. Similarly, young stars at $z = 0.1$ form in the shape of a disk and remain in a disk at $z = 0$.

Figure 4 provides a related examination of Thelma’s shape evolution, again in the C/A vs B/A parameter space. The upper left panel reproduces the shapes of $z = 0$ stellar populations binned by age, shown in Figure 2. As before, each age bin spans 500 Myr and is chosen to begin at the lookback times corresponding to specific simulation snapshots that we will compare to the other panels of this figure. The color bar maps to the minimum age of stars in each bin. The filled circles are connected by arrows in time, pointed from oldest to youngest age bins. The oldest shape measurement is circled in red and the youngest age bin is circled in blue. We see that the oldest populations ($\gtrsim 8$ Gyr) reside in spheroids ($C/A \sim 0.6$). The youngest stars ($\lesssim 2$ Gyr) inhabit thin disks ($C/A \sim 0.1$). Intermediate-age stars (~ 4 Gyr) reside in thicker disks ($C/A \sim 0.3$). As alluded to above, it is particularly striking that stars of all ages are very symmetric about the short axis, with $B/A \sim 0.9 - 1$.

For comparison, the top right panel of Figure 4 shows the shapes of the same stellar populations *at the time they were born*. These points reproduce the open circles in Figure 2, but are now connected as a time sequence from earliest times to latest times. This allows us to more directly track how the shapes are changing in time. As expected from the discussion above, we see that young stars at lookback times $\lesssim 4$ Gyr tend to inhabit disks. However, at intermediate lookback times and later, young stars are arranged in either spheroidal or elongated configurations. As can be inferred from the arrows connecting adjacent lookback time steps, young star shapes in Thelma tend to move within the spheroidal region for the first ~ 5 Gyr of cosmic time. They subsequently have elongated configurations for the next ~ 4 Gyr. During these early times, axis ratios deviate quite far from axisymmetry, with $B/A \sim 0.4 - 0.8$. This is striking in comparison to the shapes that those same stars inhabit at $z = 0$ (top left). Again, even though these stars are often formed in elongated or triaxial arrangements, they relax into quite round, axisymmetric configurations by the present day.

The bottom left panel of Figure 4 shows the shape of Thelma’s main progenitor over time, measured using the mass-weighted eigentensor of all stars. At $z = 0$, the mass-weighted shape is characterized as a thick disk ($C/A \sim 0.4$) and can be interpreted as a weighted average of the archaeological age bins shown in the top left panel. Compared to the young stars’ shapes, we see much less variation in overall shape of the total star population with time, as might be expected due to the averaging over a larger number of particles. Interestingly, however, even the all-star shape goes through periods of elongation. As with young stars, the main progenitor is much less axisymmetric at intermediate times than we see in intermediate-age populations at $z = 0$.

The bottom right panel presents a quasi-observable measure of shape evolution: the g -band luminosity weighted axis ratios at the same lookback times. The luminosity-shape evolution is qualitatively similar to the young stars’ shape evolution: the shapes move from mostly spheroidal at the earliest times to elongated at intermediate times. At late times, the luminosity-weighted shapes become disk-like. Interestingly, the luminosity-weighted points show some instances of extreme elongation, including one case with $B/A \sim C/A \sim 0.3$.

Before moving on to present a summary of sample-wide trends, we note that in Appendix B we provide similar plots to those shown in Figures 2 and 3 for all of our other simulations (Figures B2 - B6). For all but one of those twelve, the results are similar to those of

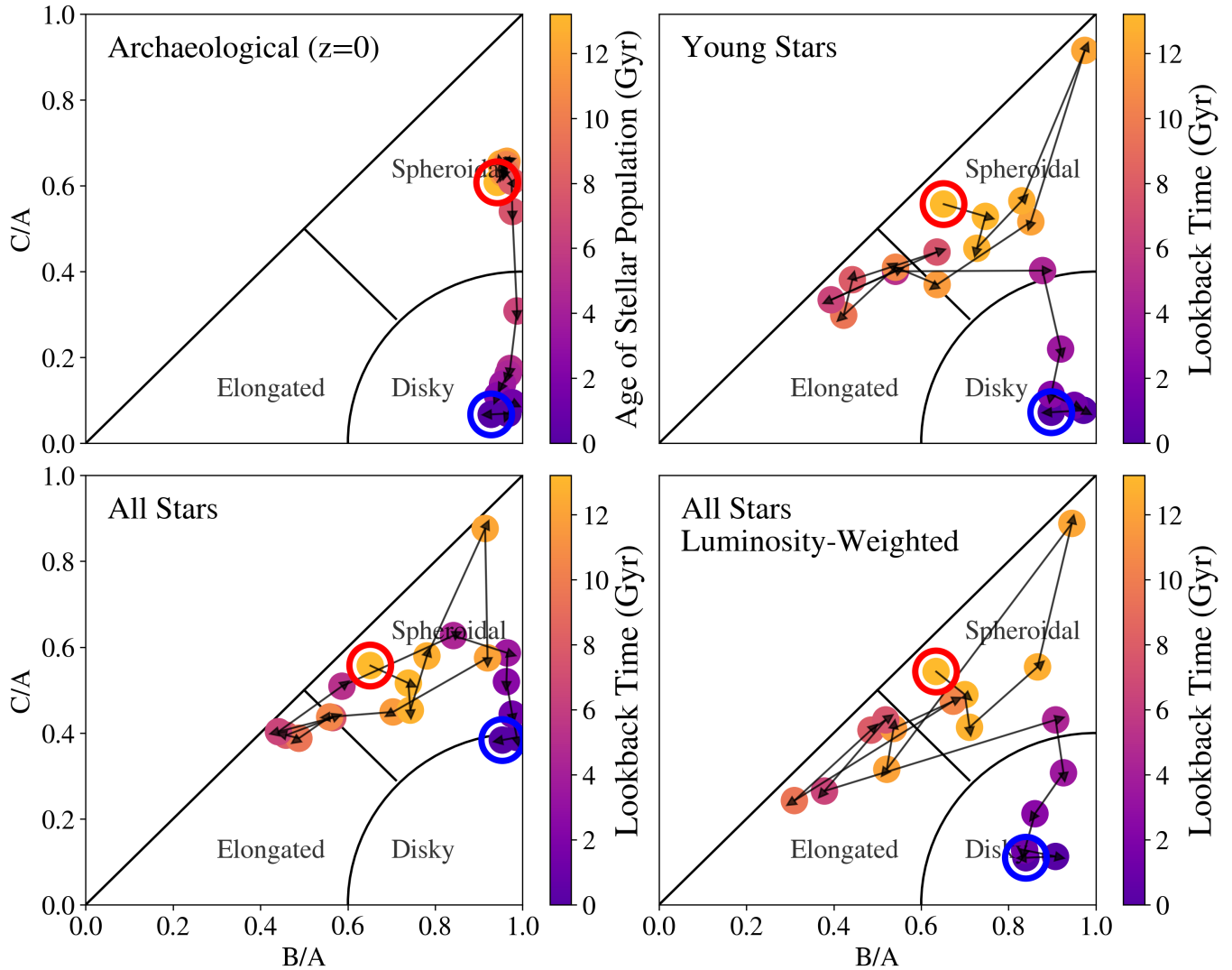


Figure 4. Shape evolution for one example Milky Way–like galaxy, Thelma. Each panel presents axis ratios as defined in §2.2 broken into the shape categories defined in Figure 1. The top left panel shows the shapes of mono-age stellar populations at $z = 0$. The color of each filled circle maps to stellar age as defined by the color bar. Beginning with the oldest population (red circle), arrows point to the next oldest age bin, up to the youngest age bin circled in blue. The top right shows the configurations of the same stellar populations at the time they were born: the axis ratios of young stars as various lookback times. The bottom left panel shows the same measurement, but now for all stars in the main progenitor at various lookback times. In the bottom right we show the shape of the main progenitor, now weighted by g -band luminosity.

Thelma. The lone exception is m12z, which is experiencing a late-time merger. For the rest, which we refer to as “Milky Way analogs,” young stars form in disks at late times, and at early times, their luminosity-weighted and mass-weighted shapes oscillated between elongated and spheroidal over $\sim 1 - 3$ Gyr timescales. The outlier, m12z, has an elongated shape at $z = 0$, driven by a merger. This may be a clue that mergers are playing a role in driving the elongated shapes that are prevalent among our sample at higher redshifts, though this is a topic that we aim to explore in a future work.

3.2. All Galaxies

Figure 5 presents a summary of the 3D shape evolution of our 13 FIRE-2 galaxies sampled at three example redshifts. The columns present shape results for our Milky Way–size galaxies ($z = 0$, right column) and their main progenitors at redshifts $z = 2$ (middle column) and $z = 4$ (left column). The color of each point in all rows maps to the total stellar mass of the galaxy at the associated redshift, as encoded by the color bars on the bottom of each row. This means that for each column, the same galaxy has the same color in all four rows.

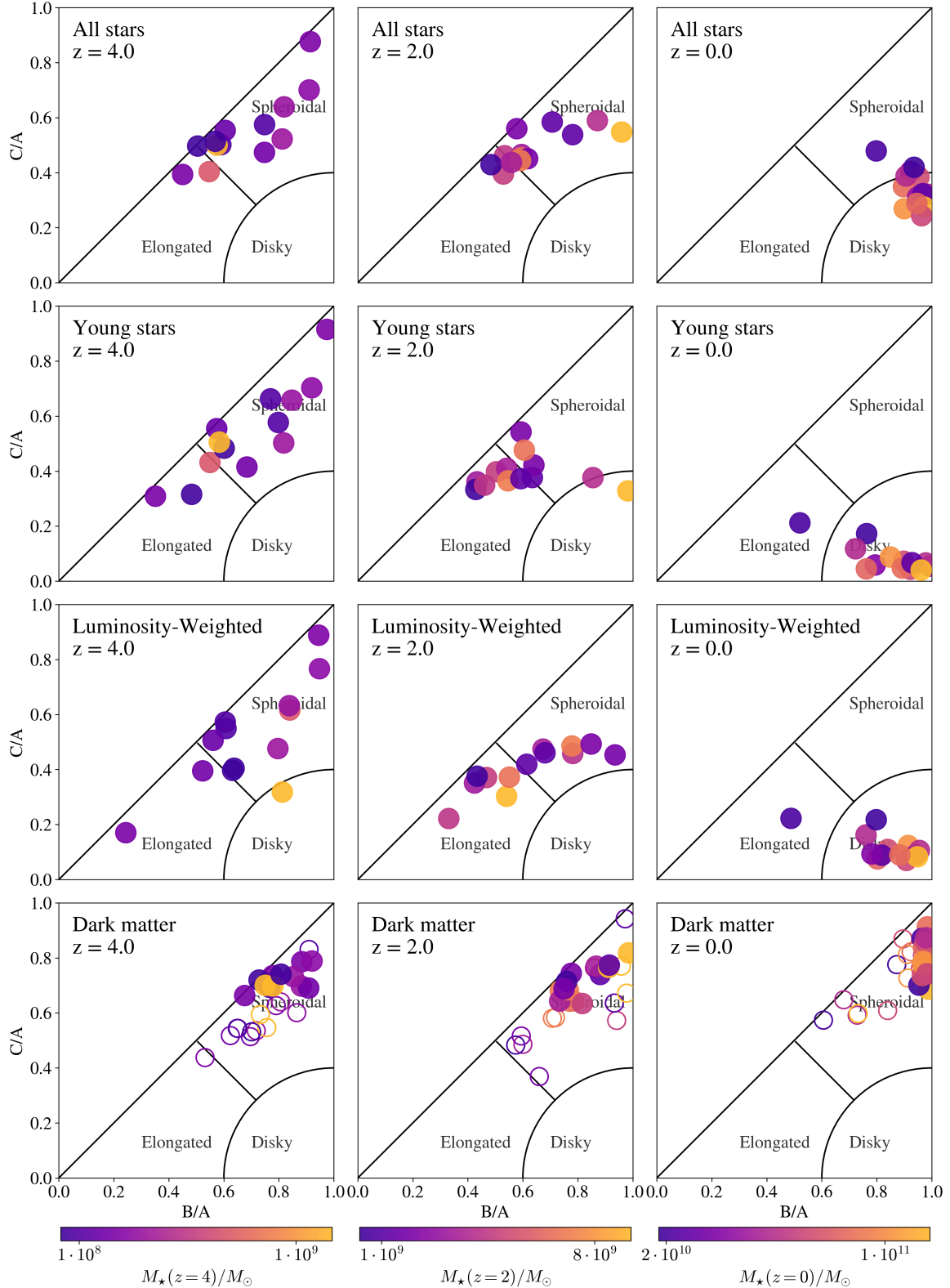


Figure 5. The 3D shape evolution of the main progenitors of all of our FIRE-2 galaxies with Milky Way masses at $z = 0$. Each panel uses the classification scheme introduced in Figure 1. The three columns show progenitor shapes at three redshifts: of $z = 4.0, 2.0,$ and 0.0 , from left to right. The rows show the shape measurements for different components: all stars (top), young stars (second), luminosity-weighted stars (third), and dark matter (bottom). The open circles in the bottom panel show dark matter shapes measured out to r_{vir} rather than our standard $0.1r_{\text{vir}}$. The color bar maps to the logarithm of the stellar mass of the all stars sample so that the same galaxy has the same color in a given column. Qualitatively, galaxy shapes tend to be more elongated or spheroidal at early times, and evolve into disk configurations at $z = 0$. The dark matter is almost always spheroidal with the exception of one point at $z = 4$.

The top row of Figure 5 presents shapes determined using all stars in the galaxy at the given redshift. At $z = 0$ (upper right), all but one galaxy has an axisymmetric ($B/A \sim 0.95$) disk ($C/A \lesssim 0.4$) configuration. Note that when the shapes are measured using all stellar mass like this, even the $z = 0$ disks are rather thick ($C/A \simeq 0.3$). The one case that is not a disk is m12z, which is one of the least massive (purple) points. This galaxy is undergoing a merger at $z = 0$. At $z = 2$ and 4, the mass-weighted shapes are typically flattened spheroids ($C/A \sim 0.5 - 0.9$, $B/A \sim 0.6 - 0.8$), although we also see that a few progenitor galaxies with elongated shapes, with $C/A \sim B/A \sim 0.4$.

The shape evolution for young stars (second row in Figure 5) is much more dramatic. At $z = 0$, young stars tend to reside in very thin disks, with $C/A \sim 0.1$, in all but one of our galaxies. As discussed above, the one exception is the lower-mass (purple) galaxy m12z, which is undergoing a merger, and has an elongated shape in young stars. Compared to the mass-weighted shapes at $z = 0$, the young stars distribution is less symmetric about the short axis ($B/A \sim 0.7 - 0.9$) than the all-stars distributions ($B/A \sim 0.9 - 1$, top panel), even though the young stars reside in much more flattened disks ($C/A \sim 0.1$).

The young stars at $z = 2$ (second row, middle panel of Figure 5) have a dramatically different arrangement from the young stars at $z = 0$: most are elongated and none are in the form of thin disks. At $z = 4$ (left panel), young stars show a variety of shapes, from fairly spheroidal ($C/A \sim B/A \sim 1$) to very elongated ($C/A \sim B/A \sim 0.3$). Although there is variance, we do see more spheroidal configurations among the young stars at $z = 4$ than we see at $z = 2$.

The third row of Figure 5 presents our “quasi-observable” shape analysis, weighted by g -band luminosity. Qualitatively, these shapes are more similar to the young stars measurements than the all-stars configurations, but we see more variance. In particular, at $z = 2$, we see that several of the g -band shapes are fairly elongated. One progenitor of note at $z = 4$ is extremely prolate, with $C/A \sim B/A \sim 0.2$ and we even have one g -band progenitor at $z = 4$ shaped like a thick disk.

The last row of Figure 5 focuses on the shapes of the galaxies’ dark matter component. The solid points show shapes measured with our standard volume of $0.1r_{\text{vir}}$, and the open points are measured within a larger volume out to r_{vir} , for comparison. Unlike the stellar components, the inner dark matter shapes are always quite spherical. The larger scale dark matter shapes (out to r_{vir} , open) show more variance but are always within the spheroidal region with the exception of one point.

The dark matter in the vicinity of the galaxies (solid points) displays a gradual transformation from triaxial spheroids at high redshift to near-perfect spheroids at lower redshifts, with $B/A \sim 1$. We do not see a systematic correlation between the elongation of dark matter shapes and the elongation of stellar populations, except for the most extreme objects at $z = 4$ (light purple, m12f) and $z = 0$ (dark purple, m12z), where the virial-radius shapes are also the most extreme. For the case of m12z, we know that this is a merger.

4. DISCUSSION AND CONCLUSIONS

We have studied the 3D structure of Milky Way–like galaxies simulated with FIRE-2 physics using a triaxial ellipsoid approximation to characterize their shapes. Of the thirteen galaxies in our sample, twelve form disks at $z = 0$. The one exception has a merger at late times. We refer to the non-merging galaxies as “Milky Way analogs.”

We find that all of our galaxies go through phases in the early Universe when they were either spheroidal or elongated (like a pickle). During these early periods, their relative axis ratios vary significantly over Gyr timescales and usually transition from spheroidal at the earliest times to elongated at intermediate times, though there is significant variance (see Figures 4 and B5). We find that these general trends hold whether we measure shapes weighted by stellar mass or stellar luminosity, though the elongation is more significant when weighted on luminosity.

We also studied how the shapes of stellar populations change from the time of their formation to their final configurations at $z = 0$. As illustrated in Figures 2, 3, and B3, stellar populations at $z = 0$ have shapes that change systematically with age: the youngest stars inhabit thin disks, intermediate-age stars have thick-disk configurations, and the oldest stars reside in flattened spheroids. In all of our Milky Way analogs, the $z = 0$ populations are symmetric about their minor axes, with intermediate-to-major-axis ratios $B/A \sim .9$. These $z = 0$ shapes are drastically different from the shapes those same stellar populations had at the time of their formation (Figures 4 and B4). In particular, early-forming populations tended to have either triaxial-spheroidal or elongated shapes at birth. The implication is that these populations change shape significantly over cosmic time. Early elongated configurations, in particular, are not stable over a Hubble time.

In previous work (Klein et al. 2025), we studied the 3D shapes of FIREbox galaxies at $z = 0$ and found that young stars tended to be oriented in elongated or spherical configurations in galaxies of stellar mass $\sim 10^{9.5}$

M_{\odot} and in disk configurations in galaxies with stellar masses $\sim 10^{10.5} M_{\odot}$. These characteristic mass ranges are broadly consistent with our results, with the caveat that all of our galaxies are $\sim 10^{10.5}$ at $z = 0$ (when they are disks) and $\sim 10^{9.5} M_{\odot}$ at $z \sim 2$ (when they are elongated or spheroidal).

One of the major takeaways from this analysis is that the elongated phase in Milky Way evolution is transient. Past work by Ceverino et al. (2015) and Tomassetti et al. (2016) also showed that elongation phases occurred in their Vela simulations ($z \gtrsim 1$) in the range of similar stellar mass. Importantly, they also found that the elongation phase was transient. In their work, the elongation occurred when galaxies were dark-matter dominated and when the dark-matter halo was also elongated and aligned with the stars. They suggested that these configurations originated from assembly along a large-scale filament; subsequent mergers and baryon domination puffed up the system to become more spherical at late times. Although a detailed exploration of the origin of the elongation phases in our simulation will be reserved for future work, it is interesting to note that we do not see a strong correlation in the inner dark-matter shape and stellar shapes among our elongated galaxies (see the bottom panels of Figure 5). One possibility is that the feedback in FIRE-2 has a stronger effect on the inner dark-matter shapes than in the Vela simulations, wiping out any correlation that might otherwise exist. However, the idea that a preferential merger axis may drive the observed elongation shapes is consistent with the fact that our only galaxy that is elongated at $z = 0$ is m12z, which experienced a late-time merger.

An important goal going forward is to understand the physical drivers of elongation in galaxies, and to

ask whether those drivers are always the same from galaxy to galaxy. As noted above, Tacchella et al. (2016) showed that their elongated systems tended to be supported by an anisotropic velocity dispersion driven by accretion along a filament. It will be interesting to ask whether this is ubiquitous among our systems. In particular, we note that in a minority of cases (see, e.g., Figure 2) there are stellar populations that are born with elongated shapes but end up in thick disk configurations at $z = 0$. This suggests that there may have been significant angular momentum or bar-like rotation near the time of formation in some cases. The answers to this and other related questions will be important as we continue to piece together an accurate picture of Milky Way assembly and galaxy evolution more generally.

ACKNOWLEDGMENTS

LYX and JSB are supported by NSF grant AST-1910965 and NASA grant 80NSSC22K0827. CK is supported by a National Science Foundation (NSF) Graduate Research Fellowship Program under grant DGE-1839285. MBK acknowledges support from NSF grants AST-1910346, AST-2108962, and AST-2408247; NASA grant 80NSSC22K0827; HST-GO-16686, HST-AR-17028, HST-AR-17043, JWST-GO-03788, and JWST-AR-06278 from the Space Telescope Science Institute, which is operated by AURA, Inc., under NASA contract NAS5-26555; and from the Samuel T. and Fern Yanagisawa Regents Professorship in Astronomy at UT Austin. LYX thanks CK and JSB for their stellar mentorship. LYX also thanks Emmeline Kim, Bryan Nnadi, James Buda, Marco Cheng, and Lily Chen for their comments and suggestions.

APPENDIX

A. EXAMPLE OF SHAPE CATEGORIES

Figure A1 shows examples of our three shape classifications. We show young stars in the main progenitor of the galaxy Thelma at $z = 4$ (spheroidal, left column), $z = 2$ (elongated, middle), and $z = 0$ (disky, right). These redshifts translate to lookback times 12.2 Gyr, 6.4 Gyr, and 1.3 Gyr, respectively. Each row shows a 2D histogram along a given projection, with a 5 kpc scale bar for reference. The top row is projected along the long axis (A) and lists the short-to-middle axis ratio (C/B) for the young stars at the associated redshift. The middle row is projected along the middle axis (B) and lists the short-to-long axis ratio (C/A). Finally, the bottom panel shows the short-axis projection (C) and

lists the middle-to-long ratio (B/A). At $z = 4$ (left), the young stars are arranged in a spheroidal configuration; each panel from top to bottom has roughly the same shape: $C/B \sim C/A \sim B/A \sim 0.95$. At $z = 2$ (middle), the young stars are elongated. The long-axis projection (top) is axisymmetric ($C/B \sim 0.85$), while the middle and short-axis projections are elongated ($C/A \sim B/A \sim 0.35$). Finally, at $z = 0$ (right) the young stars are forming in a thin, axis-symmetric disk ($C/B \sim C/A \sim 0.1$, $B/A \sim 0.9$).

B. MEASUREMENTS OF THE OTHER 12 GALAXIES

This appendix shows the shape evolution of the other 12 Milky Way–like galaxies besides Thelma, which was

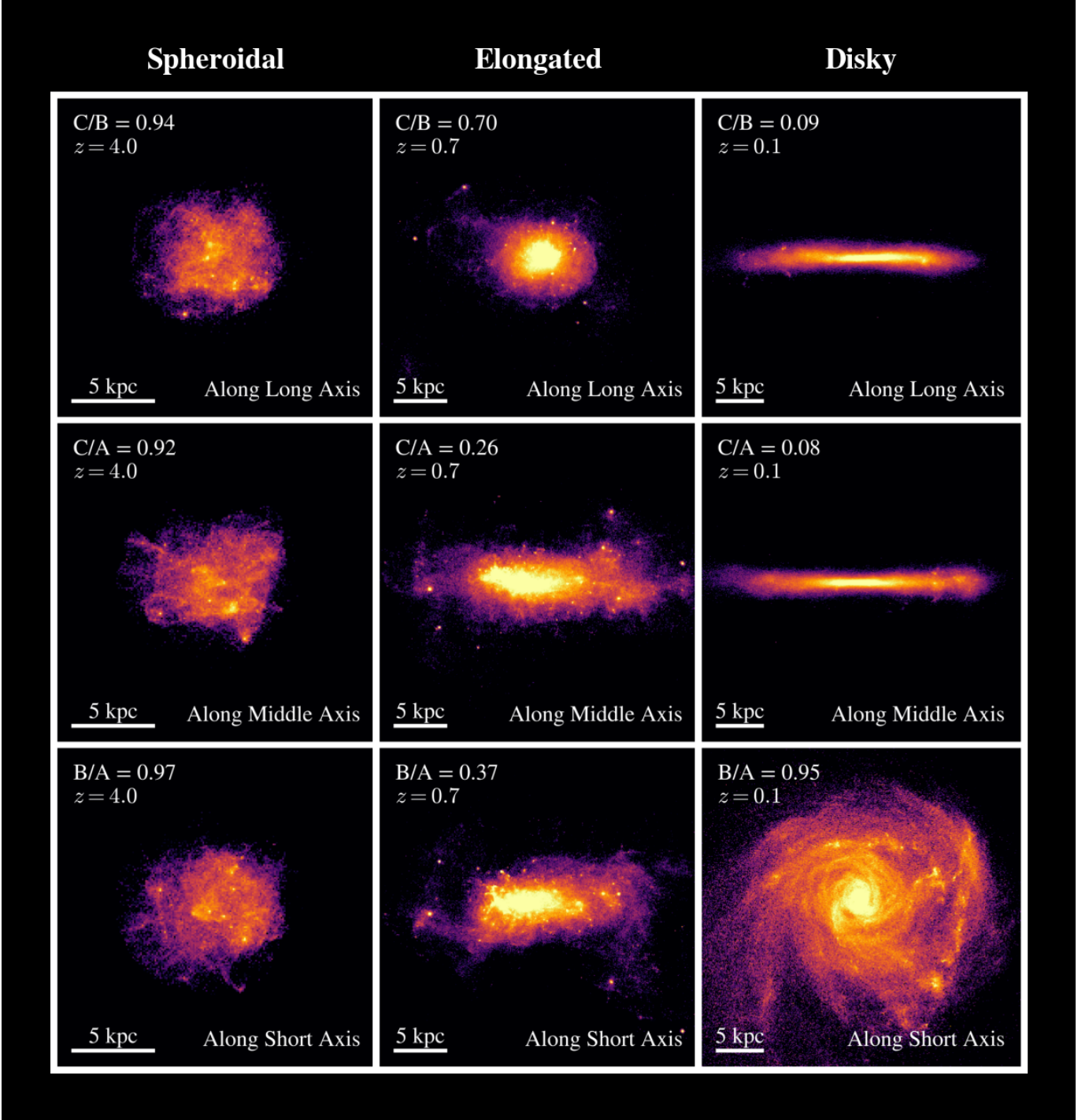


Figure A1. Illustration of our three shape classifications using young stars in Thelma at three example times from left to right: spheroidal at $z = 4$, elongated at $z = 0.7$, and diskly at $z = 0.1$. Each row shows a projection along a different axis. The top row projects each system along long axis and shows a 2D histogram of young stars in the short-to-middle plane (C vs. B). The associated C/B axis ratio is listed in each panel. The middle row projects each system along the middle axis and shows the C/A axis ratio. The bottom row projects along the short axis and lists B/A . The spheroidal example (left column) looks similar in all projections. The elongated example (middle column) looks similar along the middle and short axis projections. The disk example looks similar in the long and short axis projections.

shown in Figures 2 4. The figure shows how the shapes of stellar populations change from birth to the present day (B2). The archaeological decomposition for each galaxy is shown in Figure B3. The next figures show the shape evolution using all stars (B6), young stars (B4), and luminosity-weighted all stars (B5), respectively.

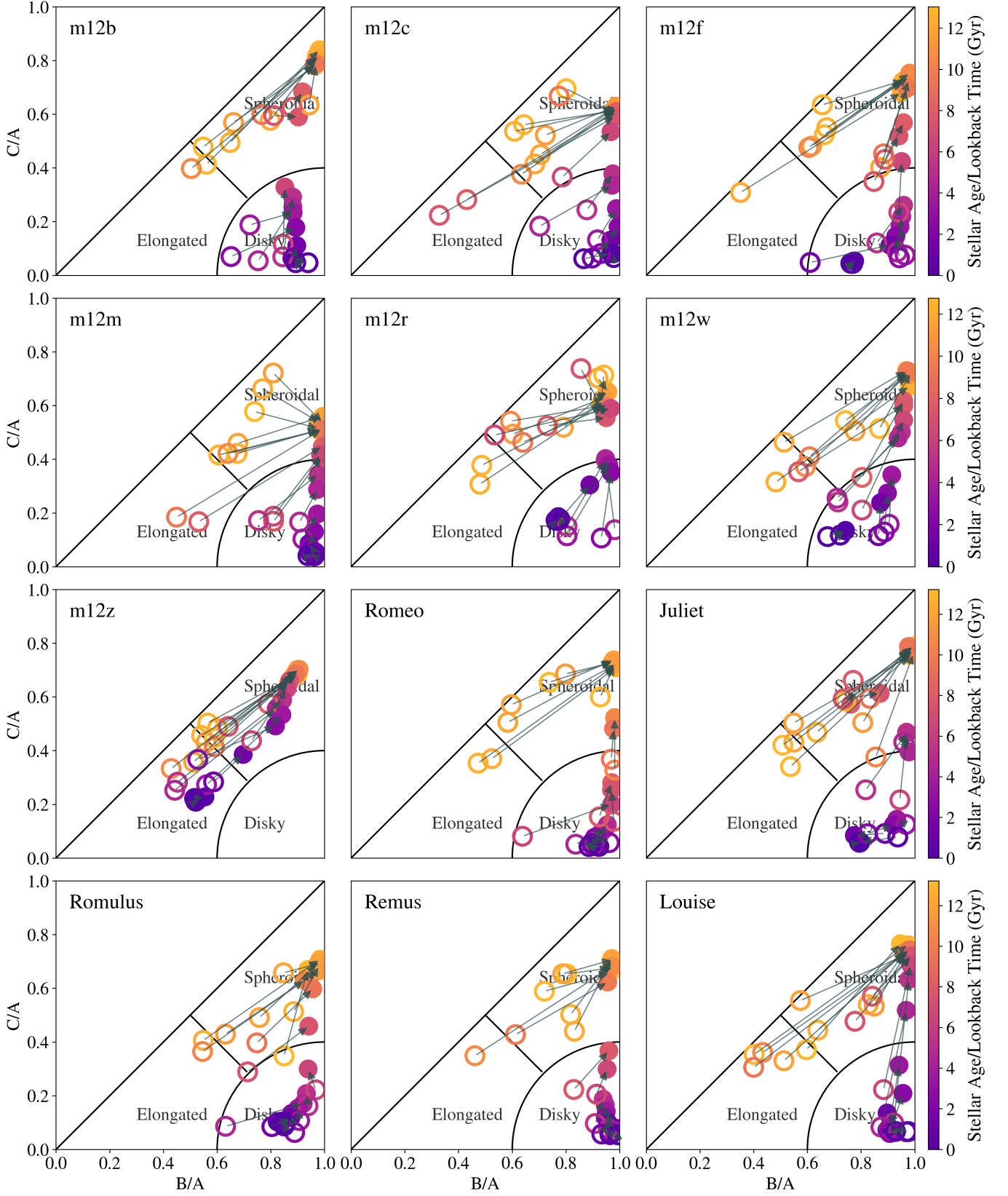


Figure B2. This figure uses the parameter space introduced in Figure 1 and mimics the presentation provided for Thelma in Figure 2 for the remaining 12 galaxies in our sample. The solid points depict the axis ratios of $z=0$ stellar populations binned by age (color bar). The open circles show the shapes of those stellar populations at their formation times. We see evolution towards symmetry about the minor axis ($B/A \sim 1$) in all cases except for m12z, which is experiencing a major merger at $z=0$.

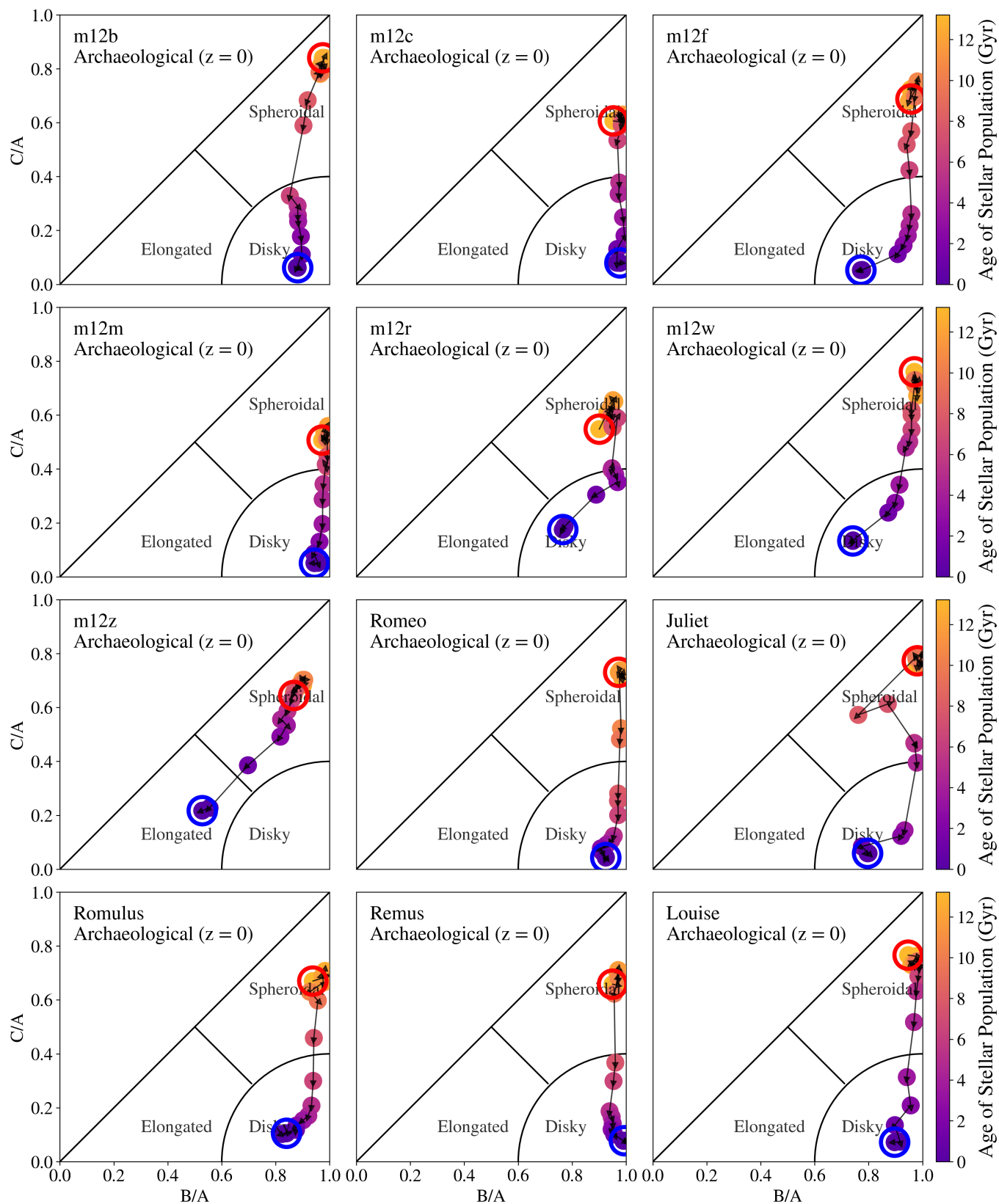


Figure B3. Archaeological decomposition of simulated galaxies, mimicking the top left panel of Figure 4. The arrows connect points in time (color bar), starting with the earliest timestep. With the exception of m12z, which is undergoing a merger, they all exhibit similar behavior to Thelma in Figure 4: stars inhabit progressively thinner disks (progressively smaller C/A) as the populations become younger. All populations have symmetric shapes about their minor axes (high B/A ratios).

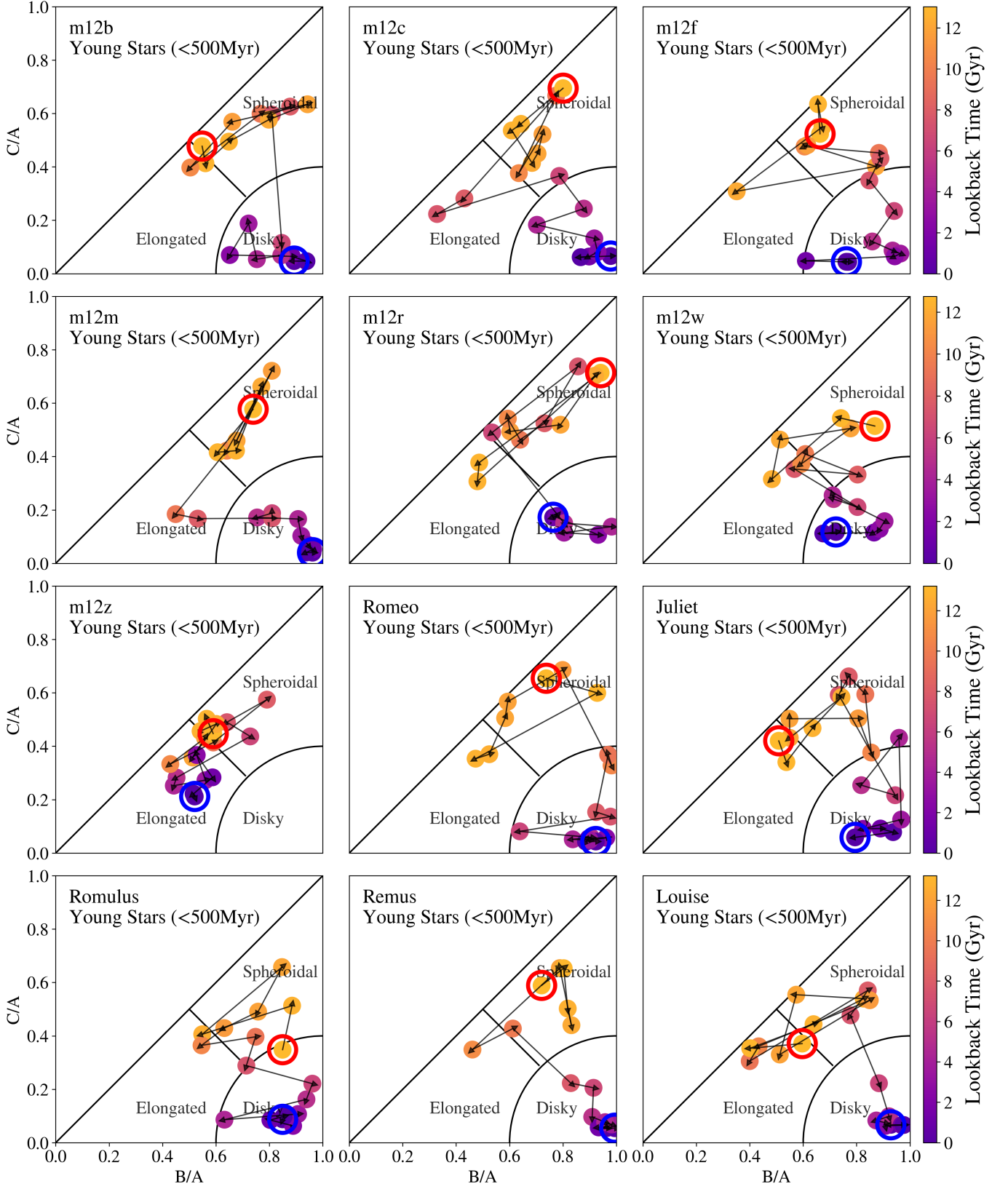


Figure B4. The young stars shape evolution of simulated galaxies, corresponding to the top right panel of Figure 4. Every galaxy goes through an elongated phase and a spheroidal phase at some point in the early Universe. In every case except m12z, which undergoes a late-time merger, young stars form disks as we approach the present day.

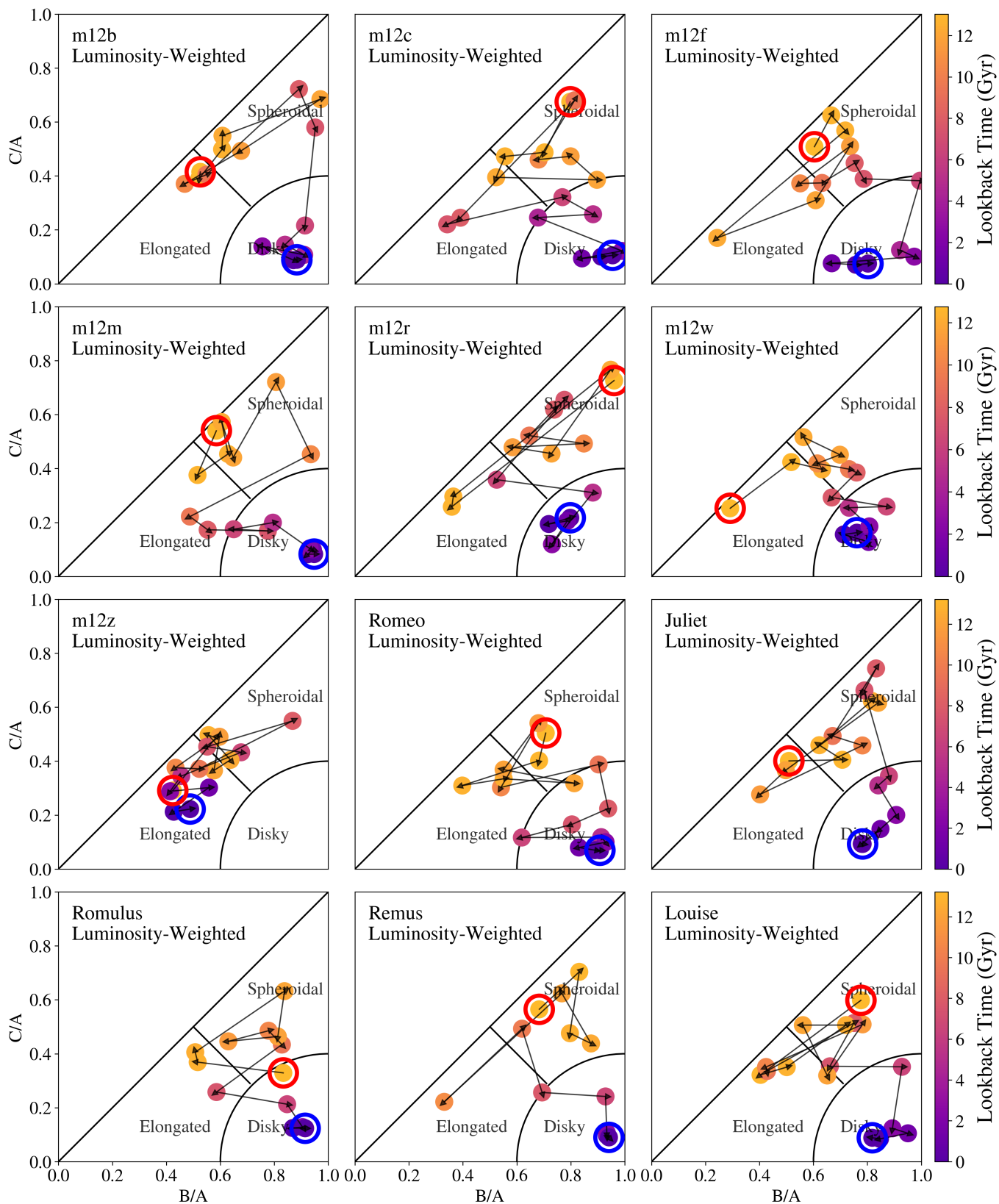


Figure B5. The luminosity weighted shape evolution of simulated galaxies, corresponding to the bottom left panel of Figure 4.

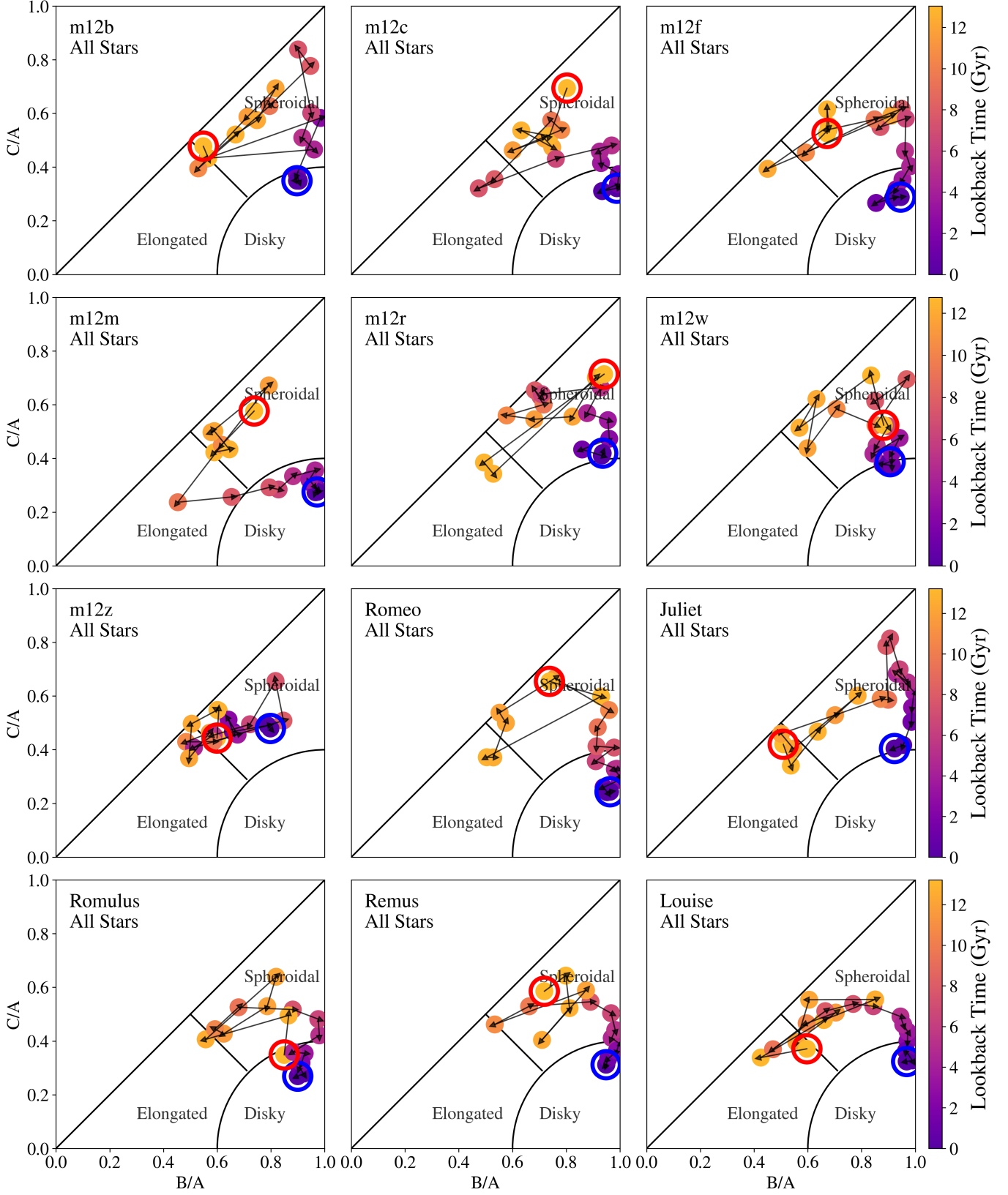


Figure B6. The all stars shape evolution of the sample, corresponding to the bottom right panel of Figure 4. Note that m12z has experienced a recent merger. It is the only galaxy that does not form a disk.

REFERENCES

- Allgood, B., Flores, R. A., Primack, J. R., et al. 2006, *MNRAS*, 367, 1781, doi: [10.1111/j.1365-2966.2006.10094.x](https://doi.org/10.1111/j.1365-2966.2006.10094.x)
- Arora, A., Garavito-Camargo, N., Sanderson, R. E., et al. 2025, arXiv e-prints, arXiv:2504.20133, doi: [10.48550/arXiv.2504.20133](https://doi.org/10.48550/arXiv.2504.20133)
- Bailin, J., & Steinmetz, M. 2005, *ApJ*, 627, 647, doi: [10.1086/430397](https://doi.org/10.1086/430397)
- Binggeli, B., & Popescu, C. C. 1995, *A&A*, 298, 63
- Binney, J. 1978, *MNRAS*, 183, 779, doi: [10.1093/mnras/183.4.779](https://doi.org/10.1093/mnras/183.4.779)
- Binney, J., & de Vaucouleurs, G. 1981, *MNRAS*, 194, 679, doi: [10.1093/mnras/194.3.679](https://doi.org/10.1093/mnras/194.3.679)
- Blumenthal, G. R., Faber, S. M., Primack, J. R., & Rees, M. J. 1984, *Nature*, 311, 517, doi: [10.1038/311517a0](https://doi.org/10.1038/311517a0)
- Bovy, J., Rix, H.-W., Schlafly, E. F., et al. 2016, *ApJ*, 823, 30, doi: [10.3847/0004-637X/823/1/30](https://doi.org/10.3847/0004-637X/823/1/30)
- Bryan, G. L., & Norman, M. L. 1998, *ApJ*, 495, 80, doi: [10.1086/305262](https://doi.org/10.1086/305262)
- Burkert, A. 2017, *ApJ*, 838, 93, doi: [10.3847/1538-4357/aa671c](https://doi.org/10.3847/1538-4357/aa671c)
- Ceverino, D., Primack, J., & Dekel, A. 2015, *MNRAS*, 453, 408, doi: [10.1093/mnras/stv1603](https://doi.org/10.1093/mnras/stv1603)
- Chua, K. T. E., Pillepich, A., Vogelsberger, M., & Hernquist, L. 2019, *MNRAS*, 484, 476, doi: [10.1093/mnras/sty3531](https://doi.org/10.1093/mnras/sty3531)
- Conselice, C. J. 2014, *ARA&A*, 52, 291, doi: [10.1146/annurev-astro-081913-040037](https://doi.org/10.1146/annurev-astro-081913-040037)
- de Nicola, S., Saglia, R. P., Thomas, J., et al. 2022, *ApJ*, 933, 215, doi: [10.3847/1538-4357/ac7463](https://doi.org/10.3847/1538-4357/ac7463)
- Elmegreen, B. G., Elmegreen, D. M., Ravindranath, S., & Coe, D. A. 2007, *The Astrophysical Journal*, 658, 763, doi: [10.1086/511058](https://doi.org/10.1086/511058)
- Elmegreen, D. M., Elmegreen, B. G., Rubin, D. S., & Schaffer, M. A. 2005, *The Astrophysical Journal*, 631, 85, doi: [10.1086/432435](https://doi.org/10.1086/432435)
- Fasano, G., & Vio, R. 1993, *Monthly Notices of the Royal Astronomical Society*, 262, 627, doi: [10.1093/mnras/262.3.627](https://doi.org/10.1093/mnras/262.3.627)
- Faucher-Giguère, C.-A., Lidz, A., Zaldarriaga, M., & Hernquist, L. 2009, *ApJ*, 703, 1416, doi: [10.1088/0004-637X/703/2/1416](https://doi.org/10.1088/0004-637X/703/2/1416)
- Favaro, J., Courteau, S., Comerón, S., & Stone, C. 2025, *ApJ*, 978, 63, doi: [10.3847/1538-4357/ad932e](https://doi.org/10.3847/1538-4357/ad932e)
- Ferguson, H. C., Dickinson, M., Giavalisco, M., et al. 2004, *ApJL*, 600, L107, doi: [10.1086/378578](https://doi.org/10.1086/378578)
- Förster Schreiber, N. M., Genzel, R., Bouché, N., et al. 2009, *The Astrophysical Journal*, 706, 1364, doi: [10.1088/0004-637X/706/2/1364](https://doi.org/10.1088/0004-637X/706/2/1364)
- Garrison-Kimmel, S., Wetzel, A., Bullock, J. S., et al. 2017, *MNRAS*, 471, 1709, doi: [10.1093/mnras/stx1710](https://doi.org/10.1093/mnras/stx1710)
- Garrison-Kimmel, S., Hopkins, P. F., Wetzel, A., et al. 2019a, *MNRAS*, 487, 1380, doi: [10.1093/mnras/stz1317](https://doi.org/10.1093/mnras/stz1317)
- Garrison-Kimmel, S., Wetzel, A., Hopkins, P. F., et al. 2019b, *MNRAS*, 489, 4574, doi: [10.1093/mnras/stz2507](https://doi.org/10.1093/mnras/stz2507)
- Haywood, M., Di Matteo, P., Lehnert, M. D., Katz, D., & Gómez, A. 2013, *A&A*, 560, A109, doi: [10.1051/0004-6361/201321397](https://doi.org/10.1051/0004-6361/201321397)
- Hopkins, P. F. 2017, *MNRAS*, 466, 3387, doi: [10.1093/mnras/stw3306](https://doi.org/10.1093/mnras/stw3306)
- Hopkins, P. F., Wetzel, A., Kereš, D., et al. 2018, *Monthly Notices of the Royal Astronomical Society*, 480, 800, doi: [10.1093/mnras/sty1690](https://doi.org/10.1093/mnras/sty1690)
- Hubble, E. P. 1926, *ApJ*, 64, 321, doi: [10.1086/143018](https://doi.org/10.1086/143018)
- Ichikawa, S.-I. 1989, *AJ*, 97, 1600, doi: [10.1086/115101](https://doi.org/10.1086/115101)
- Jurić, M., Ivezić, Ž., Brooks, A., et al. 2008, *ApJ*, 673, 864, doi: [10.1086/523619](https://doi.org/10.1086/523619)
- Kado-Fong, E., Greene, J. E., Huang, S., et al. 2020, *ApJ*, 900, 163, doi: [10.3847/1538-4357/abacc2](https://doi.org/10.3847/1538-4357/abacc2)
- Keith, B., Munshi, F., Brooks, A. M., et al. 2025, arXiv e-prints, arXiv:2501.16317, doi: [10.48550/arXiv.2501.16317](https://doi.org/10.48550/arXiv.2501.16317)
- Klein, C., Bullock, J. S., Xia, L., et al. 2025, arXiv e-prints, arXiv:2503.05612, doi: [10.48550/arXiv.2503.05612](https://doi.org/10.48550/arXiv.2503.05612)
- Lambas, D. G., Maddox, S. J., & Loveday, J. 1992, *MNRAS*, 258, 404, doi: [10.1093/mnras/258.2.404](https://doi.org/10.1093/mnras/258.2.404)
- Merritt, D., & Valluri, M. 1996, *ApJ*, 471, 82, doi: [10.1086/177955](https://doi.org/10.1086/177955)
- Padilla, N. D., & Strauss, M. A. 2008, *Monthly Notices of the Royal Astronomical Society*, 388, 1321, doi: [10.1111/j.1365-2966.2008.13499.x](https://doi.org/10.1111/j.1365-2966.2008.13499.x)
- Pandya, V., Zhang, H., Huertas-Company, M., et al. 2024, *ApJ*, 963, 54, doi: [10.3847/1538-4357/ad1a13](https://doi.org/10.3847/1538-4357/ad1a13)
- Putko, J., Sánchez Almeida, J., Muñoz-Tuñón, C., et al. 2019, *ApJ*, 883, 10, doi: [10.3847/1538-4357/ab365a](https://doi.org/10.3847/1538-4357/ab365a)
- Ravindranath, S., Giavalisco, M., Ferguson, H. C., et al. 2006, *ApJ*, 652, 963, doi: [10.1086/507016](https://doi.org/10.1086/507016)
- Rong, Y., Dong, X.-Y., Puzia, T. H., et al. 2020, *ApJ*, 899, 78, doi: [10.3847/1538-4357/aba74a](https://doi.org/10.3847/1538-4357/aba74a)
- Roychowdhury, S., Chengalur, J. N., Karachentsev, I. D., & Kaisina, E. I. 2013, *MNRAS*, 436, L104, doi: [10.1093/mnrasl/slt123](https://doi.org/10.1093/mnrasl/slt123)
- Ryden, B. S. 2004, *The Astrophysical Journal*, 601, 214, doi: [10.1086/380809](https://doi.org/10.1086/380809)
- Sandage, A., Freeman, K. C., & Stokes, N. R. 1970, *ApJ*, 160, 831, doi: [10.1086/150475](https://doi.org/10.1086/150475)

- Somerville, R. S., & Davé, R. 2015, *Annual Review of Astronomy and Astrophysics*, 53, 51, doi: [10.1146/annurev-astro-082812-140951](https://doi.org/10.1146/annurev-astro-082812-140951)
- Sotillo-Ramos, D., Pillepich, A., Donnari, M., et al. 2022, *MNRAS*, 516, 5404, doi: [10.1093/mnras/stac2586](https://doi.org/10.1093/mnras/stac2586)
- Springel, V., White, S. D. M., Jenkins, A., et al. 2005, *Nature*, 435, 629, doi: [10.1038/nature03597](https://doi.org/10.1038/nature03597)
- Sung, E.-C., Han, C., Ryden, B. S., et al. 1998, *ApJ*, 505, 199, doi: [10.1086/306166](https://doi.org/10.1086/306166)
- Tacchella, S., Dekel, A., Carollo, C. M., et al. 2016, *Monthly Notices of the Royal Astronomical Society*, 457, 2790, doi: [10.1093/mnras/stw131](https://doi.org/10.1093/mnras/stw131)
- Thob, A. C. R., Crain, R. A., McCarthy, I. G., et al. 2019, *MNRAS*, 485, 972, doi: [10.1093/mnras/stz448](https://doi.org/10.1093/mnras/stz448)
- Tomassetti, M., Dekel, A., Mandelker, N., et al. 2016, *MNRAS*, 458, 4477, doi: [10.1093/mnras/stw606](https://doi.org/10.1093/mnras/stw606)
- Valenzuela, L. M., Remus, R.-S., Dolag, K., & Seidel, B. A. 2024, *A&A*, 690, A206, doi: [10.1051/0004-6361/202450184](https://doi.org/10.1051/0004-6361/202450184)
- van der Wel, A., Chang, Y.-Y., Bell, E. F., et al. 2014, *ApJL*, 792, L6, doi: [10.1088/2041-8205/792/1/L6](https://doi.org/10.1088/2041-8205/792/1/L6)
- Vargya, D., Sanderson, R., Sameie, O., et al. 2022, *MNRAS*, 516, 2389, doi: [10.1093/mnras/stac2069](https://doi.org/10.1093/mnras/stac2069)
- Vega-Ferrero, J., Huertas-Company, M., Costantin, L., et al. 2024, *ApJ*, 961, 51, doi: [10.3847/1538-4357/ad05bb](https://doi.org/10.3847/1538-4357/ad05bb)
- Vincent, R. A., & Ryden, B. S. 2005, *ApJ*, 623, 137, doi: [10.1086/428765](https://doi.org/10.1086/428765)
- Wetzel, A. R., Hopkins, P. F., Kim, J.-h., et al. 2016, *ApJL*, 827, L23, doi: [10.3847/2041-8205/827/2/L23](https://doi.org/10.3847/2041-8205/827/2/L23)
- White, S. D. M., & Rees, M. J. 1978, *Monthly Notices of the Royal Astronomical Society*, 183, 341, doi: [10.1093/mnras/183.3.341](https://doi.org/10.1093/mnras/183.3.341)
- Yuma, S., Ohta, K., Yabe, K., Kajisawa, M., & Ichikawa, T. 2011, *ApJ*, 736, 92, doi: [10.1088/0004-637X/736/2/92](https://doi.org/10.1088/0004-637X/736/2/92)
- Zhang, H., Primack, J. R., Faber, S. M., et al. 2019, *MNRAS*, 484, 5170, doi: [10.1093/mnras/stz339](https://doi.org/10.1093/mnras/stz339)
- Zhang, J., Wuyts, S., Witten, C., et al. 2022, *Monthly Notices of the Royal Astronomical Society*, 513, 4814, doi: [10.1093/mnras/stac1083](https://doi.org/10.1093/mnras/stac1083)